

Cavitation erosion behavior and surface morphology evolution of 316LN austenitic stainless steel in 3.5% NaCl Solution

Zhisong Shao¹, Shuaixing Wang^{1,*}, Jia Kang¹, Jijun Xin², Zheng Li¹, Nan Du¹

¹ School of Material Science and Technology, Nanchang Hangkong University, Nanchang 330063, P. R. China

² Institute of Plasma Physics, Chinese Academy of Sciences, Hefei 230031, P. R.China

*E-mail: wsxxpg@126.com

Received: 7 October 2018 / Accepted: 28 December 2018 / Published: 7 February 2019

The cavitation erosion experiments of 316LN SS in 3.5 wt% NaCl solution were done using an ultrasonic vibrator. The weight loss, surface roughness and surface morphology of 316LN SS at different cavitation erosion stages were analyzed by an analytical balance, roughness profiler, 3D video microscope and SEM. The cavitation erosion mechanism of 316LN SS was briefly discussed through the electrochemical testings when cavitation existed or not. In the cavitation erosion process of 316LN SS, the surface roughness increased linearly and then slowed down, but the cumulative weight loss and the mean corrosion depth hardly changed at initial stage and increased greatly hereafter. Under the continuous action of vacuolar collapse, grain boundaries of 316LN SS were preferentially dissolved, the pitting was simultaneously formed and then obvious peeling pits and cracks were finally present on the sample surface. Comparing to the static solutions, the corrosion current density of 316LN SS in cavitation environments was bigger, and the passive zone was also narrower. That was to say, the cavitation erosion of 316LN SS was the synergetic effect process of cavitation mechanics and electrochemical corrosion. The cavitation effect promoted the occurrence of electrochemical corrosion, and the electrochemical corrosion further enhanced the role of cavitation mechanics.

Keywords: 316LN stainless steel; cavitation erosion; surface morphology; polarization curve

1. INTRODUCTION

316LN stainless steel (SS) is an ultra-low carbon and nitrogen-contained austenitic stainless steel, which is extensively used as the candidate piping materials in AP1000 nuclear power plants because of outstanding mechanical formability, good corrosion resistance and excellent high temperature strength [1-3]. Compared to 304 SS or 316 SS, 316LN SS has a lower carbon content, making the precipitation of Cr carbides more difficult [4-5], and the addition of N greatly improves the local

corrosion resistance of stainless steels [6-8]. Lee [6] demonstrated that the nitrogen alloying reduced the metastable pitting susceptibility by increasing the pitting potential, decreasing the incidence of current transients due to the metastable pits and facilitating the repassivation rate immediately. Pujar [7] found that 316 SS showed metastable pitting signals within less than 4 h of immersion in 0.5 M NaCl solution, and stable pits appeared and continued to grow after 48 h; while metastable pits were present on 316LN SS until 48 h and were repassivated during the subsequent time. In addition, the addition of nitrogen can also increase the yield strength of 316LN SS and improve its stress corrosion cracking (SCC) resistance [1]. The appropriate nitrogen content ($\sim 0.08\%$) can also improve the intergranular corrosion resistance of 316LN SS [8]. Excepting for nitrogen, a small amount of Nb and Mo in 316LN SS can also inhibit the precipitation of $\epsilon\text{-Cr}_2\text{N}$ phase and Cr_{23}C_6 phase to some extent, thereby reducing the damage of intergranular corrosion [5, 9]. Based on the above characteristics, the design life of the main pipeline for AP1000 nuclear power plant may be estimated to be extended from 40 a to 60 a, if 316LN SS is used to piping materials. However, in addition to pitting, intergranular corrosion and SCC, the 316LN SS elbow used in the AP1000 nuclear power plant may also suffer from cavitation erosion at the bends and stenosis areas. Therefore, it is necessary to study the cavitation erosion behavior of 316LN SS.

As well-known, cavitation erosion (CE) is a complicated process and generates under the interaction of mechanical, chemical, and electrochemical functions, which has many influencing factors [9-13]. The cavitation resistance of stainless steel is not only affected by its mechanical properties (such as hardness, elastoplasticity, etc.), but also closely related to the chemical composition, stability and repassivation ability of the surface passivation film [10-13]. Many studies have revealed that the passivation films on austenitic stainless steel (304 SS, 316 SS, et al) surface have a bilayer structure, and mostly are *n*-type semiconductors [14]. The compact inner layer mainly consists of CrO_3 , while the outer layer is mainly composed of the oxides and hydroxides of Fe and Cr [15-16]. Although the passivation film of nitrogen-containing 316LN SS is still an *n*-type semiconductor [6, 17], the addition of nitrogen changes the composition of the passivation film, and N element and NH_4^+ are present in the passivation film [6, 18]. Besides, the "hysteresis loop" in the cyclic polarization curve decreased, and the repassivation ability of passivation film enhanced with the increase of nitrogen content [18]. Based on previous results, it can be inferred that the cavitation resistance of 316LN SS may be significantly different from that of 316 SS or 316L SS. However, at present, only a few literature have evaluated the cavitation erosion properties of 316LN SS with different surface treatments in Hg [19, 20]. There are not yet involved about the surface structure evolution and cavitation erosion mechanism of 316LN SS during the cavitation process.

In general, the synergy between mechanical action and corrosion effect is considered to be the basic principle of cavitation erosion [9, 12, 21-22]. However, the contribution of mechanical factors or electrochemical corrosion has bigger difference for different materials and corrosion environments. It was found that electrochemical factors play an important role in the cavitation erosion of 1Cr18Ni9Ti steel in chloride media, and cavitation promotes the anodic dissolution, but has no significant effect on the cathode process [23]. Whereas, during the cavitation erosion of duplex stainless steels in LiBr solutions, cavitation promotes the transport of substances, thereby accelerates the destruction of passivation film and the formation of localized pits [24, 25]. Therefore, it is necessary to analyze the

effect of electrochemical factor and its relationship with mechanical functions on the cavitation corrosion of 316LN SS.

In this work, the changes rule of corrosion depth, weight loss of 316LN SS in NaCl solution under cavitation effect was firstly obtained; meanwhile, the surface morphology evolution of 316LN SS during the cavitation erosion process was carefully analyzed by surface profiler, three-dimensional video microscopy and SEM. Besides, the electrochemical characteristics of 316LN SS under different cavitation erosion conditions were analyzed through electrochemical testing, in order to reveal the microscopic mechanism of CE of 316LN SS.

2. EXPERIMENTAL

2.1 Materials

316LN SS, with the chemical composition (wt.%) shown in Table 1, was used as the test material. The dimension of samples were $10 \times 10 \times 10$ mm. These samples were successively polished with SiC emery papers from 240 # to 1200#, ultrasonically cleaned in ethanol, and dried in warm air. Fig. 1 shows the XRD pattern and OM metallographic image of 316LN SS. As shown in Fig. 1, only single austenite phase containing twins is observed, no other precipitations are found at the grain boundaries [26].

Table 1. Chemical composition (wt.%) of 316LN stainless steel

Elements (wt.%)	C	Cr	Ni	Si	Mn	Mo	N	P	Co	Nb	Fe
316LN SS	0.02	16.33	12.53	0.50	1.67	2.10	0.11	0.015	0.01	0.01	Bal.

2.2 Cavitation erosion experiment

Ultrasonic cavitation test is a common method to evaluate the cavitation erosion properties of materials [9, 10, 12, 27]. In this paper, the cavitation erosion experiments of 316LN SS in 3.5 wt.% NaCl solution were done using an ultrasonic vibration apparatus, as shown in Fig. 2. The whole experiment system was composed of an ultrasonic wave generator, transducer, vibrating horn, cooling bath, electrochemical workstation and other components. The ultrasonic power, ultrasonic frequency, peak amplitude and probe diameter was 500W, 20 KHz, 50 μ m and 15.9 \pm 0.5mm, respectively. Besides, the immersing depth of the probe in the solution was 12 ± 4 mm, the distance from the probe to the sample surface was ~ 0.5 mm, the solution temperature was 25 ± 2 °C, the cavitation erosion time varied from 0 to 540 min.

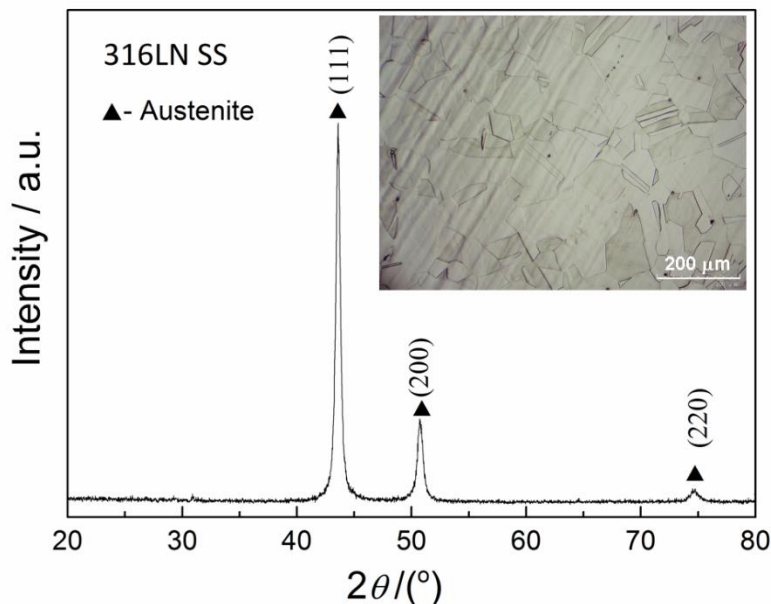


Figure 1. XRD pattern and OM metallographic image of 316LN SS.

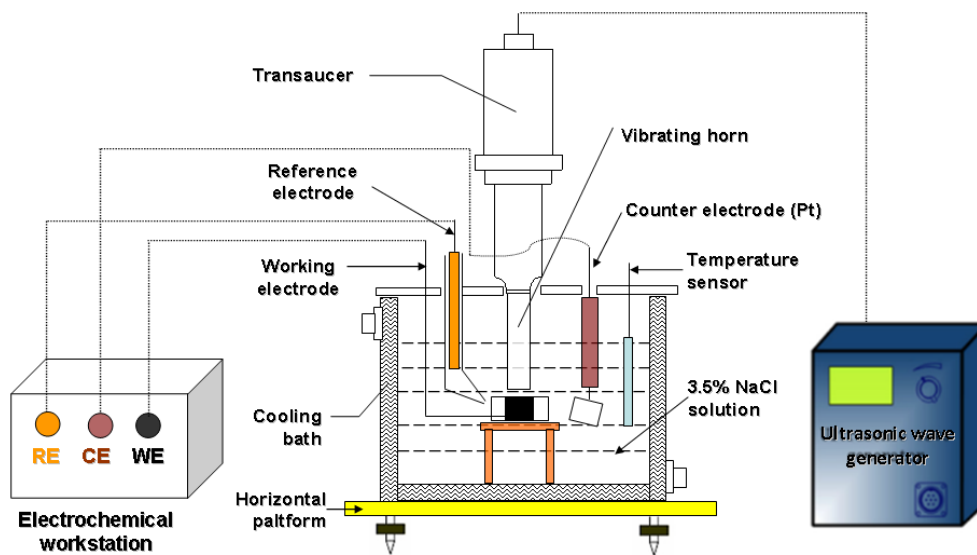


Figure 2. Schematic diagram of simulated cavitation erosion experiment system.

2.3 Electrochemical test

Electrochemical tests were performed in a three-electrode cell system using an Autolab PGSTAT 302N. Wherein, the reference electrode and the counter electrode were saturated calomel electrode (SCE) and a platinum sheet, respectively. 316LN SS sample mounted in epoxy resin, with an exposure area of 1.0 cm^2 , was used as the working electrode. The polarization curves were measured potentiodynamically from -1.0 V (vs. SCE) to 1.5 V (vs. SCE) at a scan rate of 5 mV/s . The testing solution and testing conditions was pure water and 3.5% NaCl solution on the presence or absence of

cavitation, respectively. All experiments were repeated by three duplicate specimens to confirm reproducibility of the results. The corrosion potential (E_{corr}), corrosion current density (i_{corr}), pitting potential (E_b) and passive potential zone was analyzed by the Nova 1.10 software.

2.4 Characterization

The weight loss of 316LN SS during the cavitation erosion process was measured by an analytical balance (CPA 225D) with the accuracy of 0.01 mg. The surface roughness (R_q) of 316LN SS was observed by using SJ-310 surface profile meter. The stylus radius and measurement accuracy was 2 μm and 0.001 μm , respectively. When the erosion profile was measured, the sampling trajectory passed through the center of cavitation-erosion zone and the sampling length was 18 mm to ensure the maximum profile. The 3D profile morphology of 316LN SS were observed by a KH-7700 three-dimensional microscope. The micro-morphology and phase structure of 316LN SS was analyzed by a field emission gun SEM (FE-SEM, Nova Nano SEM 450) and X-ray diffraction (XRD, Bruker D8-Advance), respectively.

3. RESULTS AN DISCUSSION

3.1 Weight loss and roughness changes of 316LN SS in cavitation erosion process

Fig. 3a shows the cumulative weight loss of 316LN SS in NaCl solution during cavitation erosion process. It was seen that the weight loss of 316LN SS gradually increased with the increase of cavitation time, but the growth rate of weight loss at different stages had significant differences. In the initial stage (0-180 min), the cumulative weight loss only had minor changes; but the weight loss increased linearly hereafter. Fig. 3b gives the roughness distribution on the surface of 316LN SS after different cavitation time. As shown in Fig. 3b, due to the influence of cavitation mechanics, the obvious cavitation-erosion zones developing along the longitudinal direction were present on the sample surface. Besides, as the cavitation time increased, the surface damage area enlarged and the degree of concavity became more pronounced. In particular, the cavitation-erosion zones of 316LN SS showed obvious pits at 360 min ~ 540 min.

In addition, the R_q values were calculated according to the 2D profile curves, and the mean corrosion depths were measured, as shown in Fig. 4. It was seen that the mean corrosion depth hardly changed in the initial stage and increased greatly after 180 min, which was consistent with the variation of weight loss. However, R_q first increased linearly and then slowed down. According the variation of R_q , the weight loss and the mean corrosion depth, the cavitation erosion process of 316LN SS in NaCl solution could be divided into two stages. At the beginning (0-180 min), R_q increased linearly from 0.098 μm to 0.803 μm , but the weight and thickness of 316LN SS almost had no significant change in this stage. After 180 min, the growth of R_q slowed down, the weight loss and the mean corrosion depth increased greatly. The cumulative weight loss increased to 9.5 mg at 540 min, which was about 10 times of that in the initial stage.

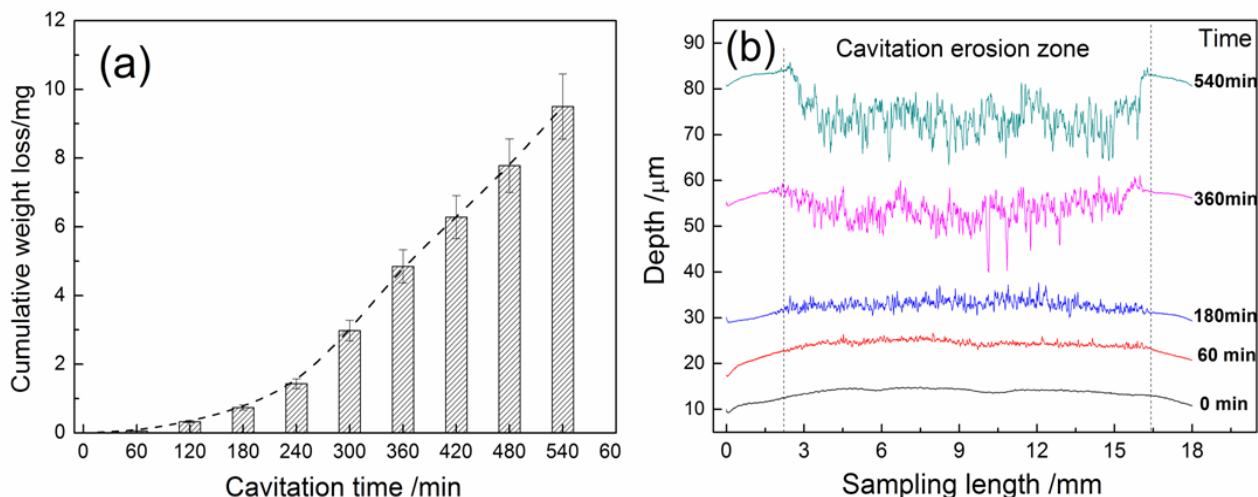


Figure 3. The cumulative weight loss (a) and two-dimensional roughness distribution of 316LN SS after different cavitation erosion time.

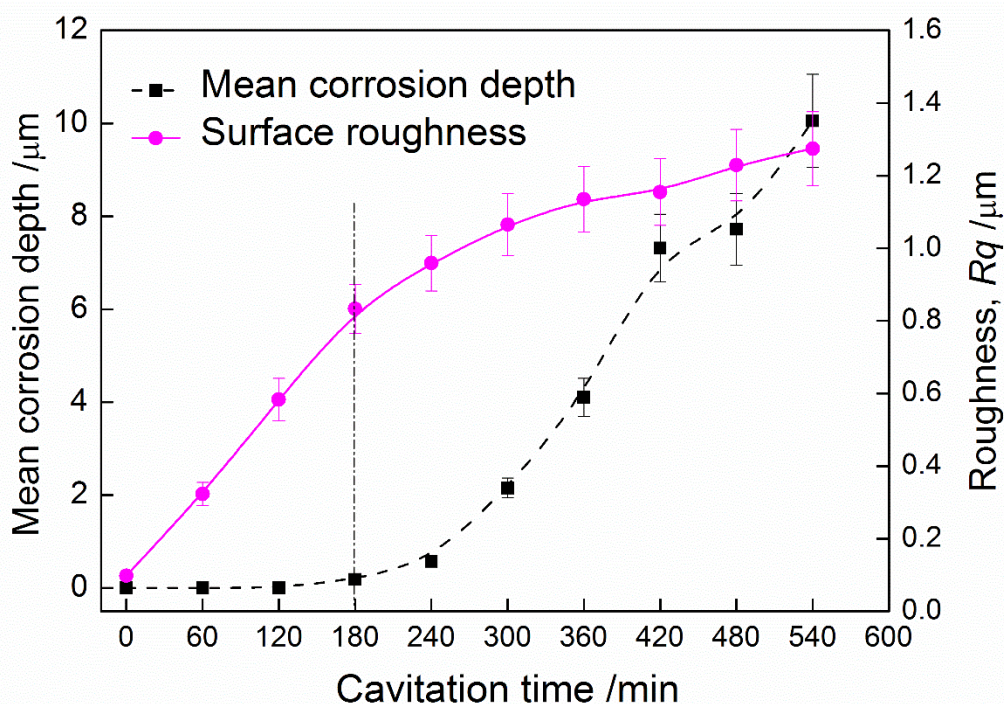


Figure 4. Mean corrosion depth and surface roughness of 316LN SS during cavitation erosion process.

In general, the surface of stainless steel firstly produced cracks and gullies under the cavitation effect [11, 13, 19, 21], but corrosion pits only occurred at the local position in the initial stage. Therefore, the corrosion depth and weight loss of 316LN SS did not change significantly from 0 to 180 min. With the continuation of cavitation, the old cracks spread and new cracks generated on the surface, many small cracks and gullies might gather into obvious concaves. Besides, the plastic deformation might be occurred on the sample surface under the cavitation mechanics [22, 28]. The uneven hardening layer on

the sample surface would result in the non-uniformity of electrochemical potential, and so the electrochemical corrosion was exacerbated. Under the above dual role, many obvious cracks were present on the surface of 316LN SS, and the partial regions peeled from the sample, as demonstrated by the higher roughness and bigger weight loss.

3.2 Surface morphology evolution of 316LN SS in cavitation erosion process

Fig. 5 shows the surface morphologies (a, b, c, d, e) and the corresponding three-dimensional topographies (f, g, h, i, j) of 316LN SS during the cavitation erosion process. The evolution of surface structure (pits, cracks and grooves) for 316LN SS could be seen directly from 2D topographies. In addition, 3D morphologies also visually displayed the depth and distribution of pits, gullies and concaves on the sample surface. Among them, the blue areas represented the concave zones formed by the exfoliation of partial material; the red areas reflected the stacking of material on the grain boundaries (GBs) under the plastic deformation.

As shown in Fig. 5a and 5f, the surface of untreated sample was flat, only a small wear marks were present. After cavitation, a series of injuries appeared on the sample surface, including pits, grooves, cracks and peeling. Moreover, the damage area and damage degree of the sample surface were intensifying with the increase of cavitation time. At 60 min, 316LN SS surface presented the apophyses of GBs (Fig. 5b), indicating that 316LN SS had undergone a slight plastic deformation under the vertical pressure from the collapse of vacuoles [22, 28]. During the deformation process, GBs could hinder the movement of dislocation and caused the stuffing of dislocations, which might create the stress concentration areas and result in the preferential damage of GBs [29-30], as demonstrated by the presence of the micro-cracks distributed along the GBs. Besides, the partial passivation film on the sample surface was damaged during cavitation, yet other regions were still relatively intact. Due to the uneven electrochemical potential, the incomplete zones may corrode as the anodes and formed small pits [17, 25, 31], as shown in Fig. 5b. However, the erosion degree of 316N SS was generally relatively slight at this moment.

As the cavitation time increased to 180 min, the plastic deformation degree of 316LN SS surface was intensified. The previous micro-cracks at GBs were continuously deepened and expanded under the cavitation mechanics, some cracks were peeled off and formed to grooves, as shown in Fig. 5c. Meanwhile, some new cracks were generated again. The 3D image (Fig. 5h) showed the distribution range and depth of concaves were significantly greater than that at 60 min. After a period of cavitation (360 -540 min), large pits, deep cracks and rugged 3D profiles were simultaneously present, indicating that the passivation film on the surface of 316LN SS was subjected to the uneven destruction of cavitation erosion [12, 25]. Now, almost all the passivation film was peeled off, and the stainless steel began to suffer serious corrosion.

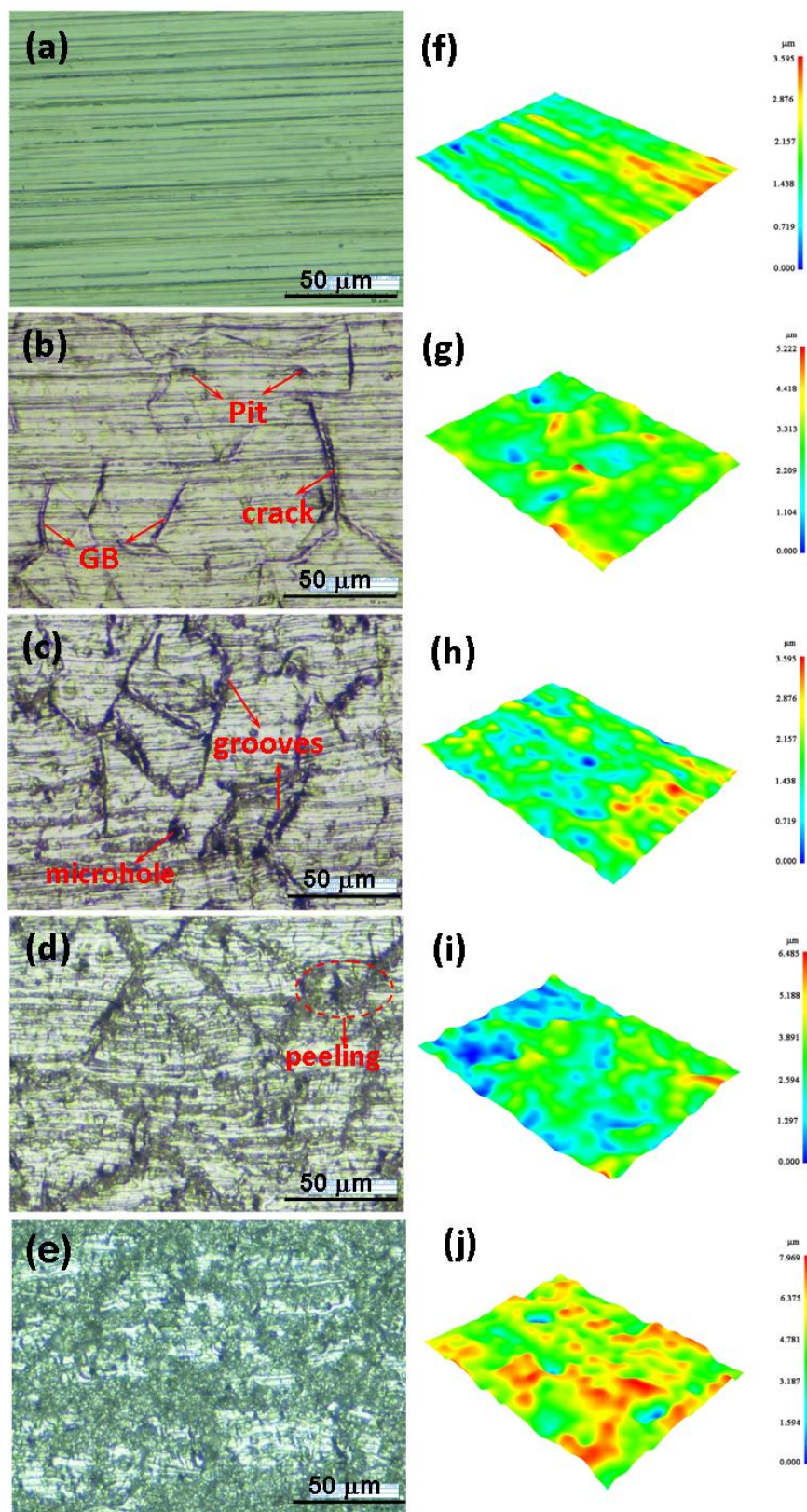


Figure 5. Surface morphologies (a, b, c, d, e) and 3D images (f, g, h, i, j) of 316LN SS after different cavitation-erosion time: (a, f) 0min; (b, g) 60 min; (c,h) 180 min; (d, i) 360min; (e, j) 540min.

3.3 Cavitation erosion characteristics of metallographic 316LN SS

In order to further analyze the beginning of cavitation erosion of 316LN SS, the samples were firstly etched in aqua region for 30 s to get metallographic appearance, hereafter, the metallographic samples were cavitation-eroded for different time, the corresponding morphologies were shown in Fig.6.

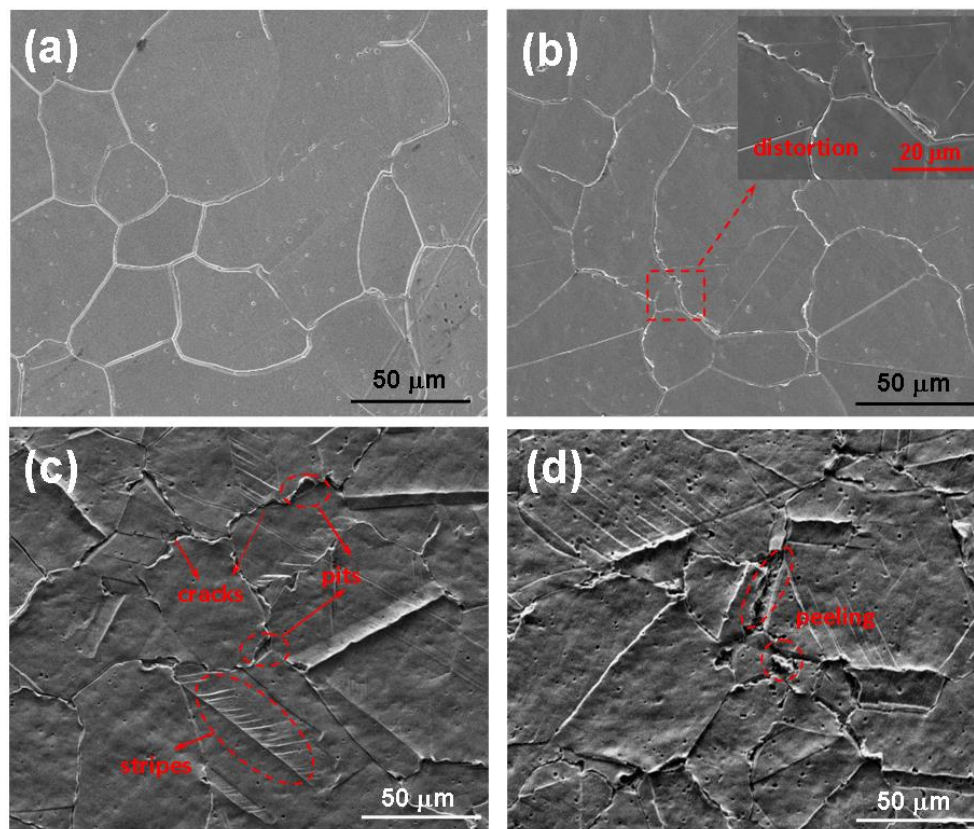


Figure 6. SEM image of metallographic 316LN SS after different cavitation-erosion time: (a) 0 min; (b) 30 min; (c) 60 min; (d) 120 min.

As shown in Fig. 1 and 6a, only a single austenite phase containing twins was observed for the un-cavitated sample, and all GBs were uniform and smooth. After cavitation for 30 min, the sample surface has begun to undergo the slight plastic deformation. From the partial magnification image in Fig. 6b, it could be found that the deformation occurred preferentially in the GBs, some GBs had been distorted, and a small amount of material was peeled off at the GBs.

When the sample was subjected to cavitation for 60 min (Fig. 6c), excepting for the deformation and uplift of GBs, the obvious rheological stripes, micro-cracks and pits were also present on the sample surface. Moreover, Fig. 6c clearly showed the distribution and details of each defect as compared to Fig. 5b. As shown in Fig. 6c, most of the rheological stripes accumulated near the GBs, which further illustrated that GBs hindered the movement of dislocation and resulted in the uplift of GBs. Besides, it could be seen that the micro-cracks were always distributed along the GBs, the pits also occurred at the GBs, which further showed that GBs were subjected to greater stress during cavitation and were first destroyed [29-30].

As the cavitation time increased, the surface damage of 316LN SS increased significantly, but the cavitation time did not change the position and mechanism of the damage. All the damages, including cracks and pits, were still distributed at/along the GBs, as shown in Fig. 6d. However, as the cavitation time increased from 60min (Fig. 6c) to 120 min (Fig. 6d), the cracks and pits nearby the GBs continued to widen and deepen, meanwhile, new pits were produced, which together resulted in the spalling of matrix material in the GBs zone, as demonstrated by the presence of annular peeling pits distributed along the GBs.

3.4. Polarization curves of 316LN SS under various cavitation-erosion conditions

In general, the corrosion resistance of stainless steel can be reflected by the characters of passivation film [6, 15-18, 31], including the passive current density (i_p), passive region range and breakdown potential (E_b), which can be effectively measured by dynamic potential polarization curve. Fig. 7 gives the dynamic potential polarization curves for 316LN SS in pure water or 3.5% NaCl solution with or without cavitation. As shown in Fig. 7, typical passivation features with a broad passive region were displayed in the anodic branch of polarization curves, regardless of the conditions. However, the passivation film properties were very different under different conditions. The specific electrochemical parameters, including corrosion current density (i_{corr}), corrosion potential (E_{corr}), i_p and E_b , were fitted by Tafel extrapolation and tabulated in Table 2. Meanwhile, Fig. 8 gives the surface corrosion morphology of 316LN SS after electrochemical testing under various conditions.

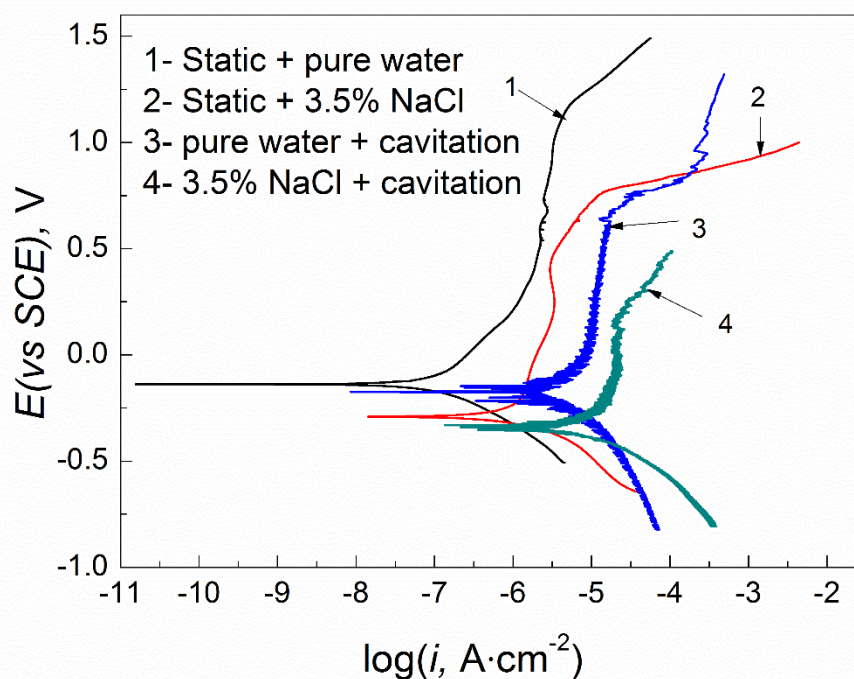


Figure 7. Polarization curves of 316LN SS under various cavitation-erosion conditions

As shown in Fig. 7, Table 2 and Fig. 8a, under static water, 316LN SS had typical passive features with a broad passive region (615 mV), the i_{corr} was only $0.085 \mu\text{A}\cdot\text{cm}^{-2}$, meanwhile, almost no change occurred on the sample surface after testing (Fig. 8a). The presence of Cl^- significantly increased the pitting sensitivity and accelerated the corrosion of 316LN SS, as demonstrated by the increase of i_{corr} , the reduction in passive region (~ 403 mV) and the decrease of E_b in the static NaCl solution. After polarization, a large number of pits and black products appeared on the electrode surface (Fig. 8c). A common explanation was that the strong penetration ability of Cl^- and its competitive adsorption with oxygen will destroy the protective effect of the passivation film, causing the passivity of stainless steel to be interrupted at potentials below E_b [31-33].

Table 2. Fitting values of polarization curves for 316LN SS under various cavitation-erosion conditions

Testing conditions	$E_{\text{corr}} / \text{V}$	$i_{\text{corr}} / \mu\text{A}\cdot\text{cm}^{-2}$	$i_p / \mu\text{A}\cdot\text{cm}^{-2}$	E_b / V	Passive Region /mV
Pure water + Static	-0.129	0.085	2.56	1.165	865
3.5%NaCl + Static	-0.298	0.447	3.37	0.706	645
Pure water + Cavitation	-0.186	1.97	10.23	0.613	603
3.5% NaCl + Cavitation	-0.347	6.75	19.49	0.169	369

When the cavitation effect was applied, although the polarization curve of 316LN SS still exhibited passive characteristics, the E_{corr} of 316LN SS under cavitation conditions had a negative shift, and the i_{corr} significantly increased in both pure water and NaCl solution. Compared with static pure water and NaCl solution, the corrosion rate of 316LN SS under cavitation conditions increased by approximately 18 times and 22 times, respectively. That was to say, cavitation obviously accelerated the corrosion of 316LN SS. Besides, the i_p of 316LN SS under cavitation conditions showed large fluctuations, indicating that the passivation film on 316LN SS surface was in meta-stable state of constant dissolving. The possible reason was that the local sites of passive film were damaged under cavitation mechanical action [17, 25], which was confirmed by Fig. 8b, small micro-cracks along GBs and a few pits were present on the 316LN SS surface under cavitation in pure water.

In addition, the cavitation erosion of 316LN SS was significantly more severe in chlorine-containing systems than cavitation in pure water. As shown in Fig. 7 and Table 2, the i_p of 316LN SS in the vibrant NaCl solution was larger and had greater fluctuations; and E_b was significantly reduced. It was believed that the cavitation mechanical action resulted in the rupture of local passivation film on the stainless steel surface (Fig. 8b), and then formed a corrosion micro-battery with large cathode-small anode. Meanwhile, the presence of Cl^- further intensified the destruction of the passivation film. Under the synergistic effect of mechanical action and Cl^- , the local sites of 316LN SS surface experienced active dissolution and formed the serious corrosion pits. Simultaneously, the obvious rheological stripes and micro-cracks were also present under this condition, as shown in Fig. 8d.

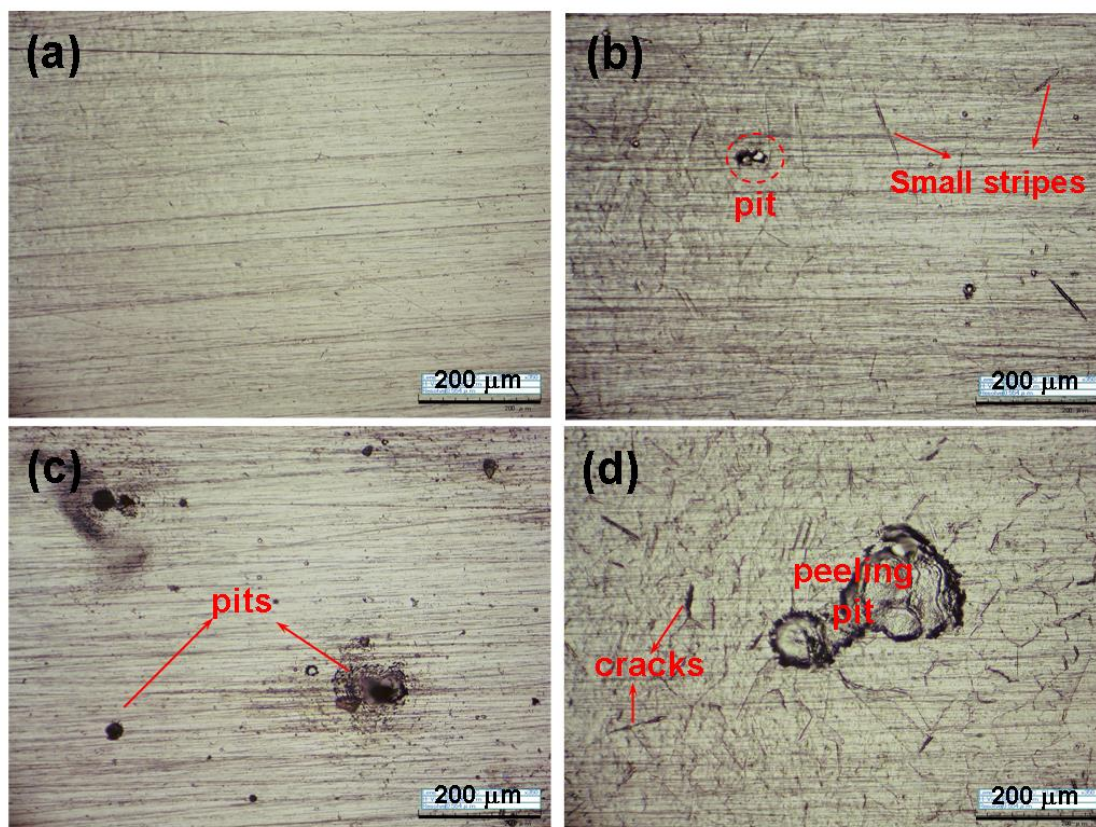


Figure 8. OM images of 316LN SS after polarization in static pure water (a), cavitation in pure water (b), static 3.5%NaCl solution (c) and cavitation in 3.5%NaCl solution (d).

3.5 Discussion of cavitation erosion mechanism of 316LN SS

Based on the average erosion depth (Fig. 3), accumulative weight loss (Fig. 3 and 4), the changes of 3D profile (Fig. 5) and micro-morphology (Fig. 6) during cavitation-erosion, the evolution process of cavitation-erosion for 316LN SS could be inferred.

In the cavitation-erosion process of 316LN SS, plastic deformation preferentially occurred at the GBs [29-30] under the impact energy generated by bubble collapse, and then multiple injuries (apophyses, cracks, pits) was present at GBs, as shown in Fig. 5b and 6c. Accordingly, the integrity of the passivation film on the electrode surface had been destroyed. The fresh substrate appeared at the grain boundaries and became the electrochemical active sites [17, 25, 31]. The active chlorine ions in the system were more likely to adsorb at these locations, thereby promoting the destruction of the passivation film. Due to the electrochemical inhomogeneous of the electrode surface, the corrosion micro-cells with small anode-large cathode were formed, and resulted in the pitting nucleation, as demonstrated by Fig. 5b and 5c.

With the progress of cavitation-erosion, the guided wave action of surface pits made the stress more concentrated, thereby enhanced the cavitation mechanical forces and aggravated the destructive effect of the cavitation process [22, 34]. Meanwhile, the corrosion products in the pits could be promptly diffused into the solution under the stirring effect of cavitation [34], and the corrosive medium was also

easily to reach the substrate surface, which resulted in the deepening and expansion of the original pits around GBs, and the generation of new cavitation pits.

Besides, the micro-jets and shock waves generated by ultrasonic cavitation forces could cause severe mechanical impact on the sample surface [35], which might result in cyclic fatigue or stress corrosion conditions on the 316LN SS surface. Continuous stress forces could intensify the damage of the GB region and caused the partial shedding of surface materia. The sample surface uniformity also changed, and then many corrosion micro-cells were formed. In other words, the combined effect of electrochemical dissolution and mechanical failure resulted in the aggravation of cavitation damage and the severe shedding of surface material, as shown in Fig. 6d. Therefore, after 180 min, the average cavitation depth and cumulative weight loss began to increase rapidly, as shown in Fig. 3 and 4. Although the cavitation erosion depth in different regions of 316LN SS surface would change due to the randomness of cavitation and the microstructure of the material, all the damage of cavitation erosion zones developed in the longitudinal direction, and the surface profile of different erosion zones were similar, as shown in Fig. 6.

In summary, it could be determined that grain boundaries of 316LN SS were preferentially dissolved during cavitation erosion, while the pitting simultaneously formed on the steel surface. The cavitation erosion continued to proceed under the combined effect of cavitation mechanical force and electrochemical corrosion factors.

4. CONCLUSION

(1) During the cavitation erosion process of 316LN SS, the surface roughness firstly increased linearly and then slowed down, but the cumulative weight loss and the mean corrosion depth hardly changed at initial and increased greatly hereafter.

(2) During the cavitation erosion process, grain boundaries of 316LN SS were preferentially plastically deformed and dissolved. At the same time, the pitting was formed, and then obvious peeling pits and cracks were finally present at the sample surface.

(3) The cavitation erosion of 316LN SS in NaCl solution was the synergetic effect process of cavitation mechanics and electrochemical corrosion. Comparing to the static solutions, cavitation obviously accelerated the corrosion of 316LN SS, as demonstrated by a sharp increase of i_{corr} and the lessening of passive zone.

ACKNOWLEDGEMENTS

The authors gratefully acknowledge the financial support of National Natural Science Foundation of China (Grant No. 51561024).

References

1. A.Poonguzhali, T. Anita, N. Sivaibharasi, H. Shaikh, R.K. Dayal, *T. Indian I. Metals*, 67 (2014) 177-184.

2. N. Sivai Bharasi, K. Thyagarajan, H. Shaikh, *J. Nucl. Mater.*, 377 (2008) 378-380.
3. H. Shaikh, T. Anita, R.K. Dayal, H. S. Khatak, *Corros. Sci.*, 52 (2010) 1146-1154.
4. II. S. Downey, K. Han, P. N. Kalu, K. Yang, Z. M. Du. *Metall. Mater. Trans. A*, 41 (2010) 881-887.
5. W. Lu, X. Hua, X. Zhou, J. Huang, X. Peng. *J. Alloys Compd.*, 701 (2017) 993-1002.
6. J. B. Lee, S. I. Yoon, *Mater. Chem. Phys.*, 122 (2010) 194-199.
7. M. G. Pujar, N. Parvathavarthini, S. S. Jena, B. V. R. Tata, R.K. Dayal, H. S. Khatak, *J. Mater. Eng. Perform.*, 17 (2008) 793-801.
8. H. Hänninen, J. Romu, R. Ilola, J. Tervo, A. Laitinen, *J. Mater. Process. Technol.*, 117 (2001) 424-430.
9. D. G. Li, D. R. Chen, P. Liang, *Ultrason. Sonochem.*, 35 (2017) 375-381.
10. Y. X. Qiao, X. Cai, C. Ouyang, Y. G. Zheng, *I. J. Electrochem. Sci.*, 11 (2016) 10329-10346.
- I. Mitelea, L. M. Micu, I. Bordeas̃u, CM Crăciunescu, *J. Mater. Eng. Perform.*, 25 (2016) 1939-1944.
11. Z. Li, J. Han, J. Lu, J. Zhou, J. Chen, *Wear*, 321 (2014) 33-37.
12. S. Hattori, R. Ishikura, *Wear*, 268 (2010) 109-116.
13. Z. Feng, X. Cheng, C. Dong, L. Xu, X. Li, *Corros. Sci.*, 52 (2010) 3646-3653.
14. C. Man, C. Dong, Z. Cui, K. Xiao, Y. Qiang, X. G. Li, *Appl. Surf. Sci.*, 427 (2018) 763-773.
15. C. Pan, L. Liu, Y. Li, S. Wang, F. Wang, *Electrochim. Acta*, 56 (2011) 7740-7748.
16. M. G. Pujar, N. Parvathavarthini, R.K. Dayal, *J. Mater. Sci.*, 42(2007) 4535-4544.
17. S. Ningshen, U. K. Mudali, V. K. Mittal, H. S. Khatak, *Corros. Sci.*, 49 (2007) 481-496.
18. S. J. Pawel, *J. Nucl. Mater.*, 343(2005) 101-115.
19. D. H. Mesa, C. M. Garzón, A. P. Tschiptschin, *Wear*, 271 (2011) 1372-1377.
20. K. H. Lo, F. T. Cheng, H. C. Man, *Mater. Sci. Eng. A*, 357(2003) 168-180.
21. R. Zhang, H. J. Shen, Y. Q. Zhang, D. L. Li, Y. J. Li, X.Y. Yong, *Acta Metall. Sin.*, 49(2013) 614-620. (in Chinese)
22. X.Y. Yong, J. Ji, Y.Q. Zhang, D. L. Li, Z. J. Zhang, *Cor. Sci. Pro. Tech.*, 23 (2011) 116-120. (in Chinese)
23. D. M. García-García, J. García-Antón, A. Igual-Muñoz, E. Blasco-Tamarit, *Corros. Sci.*, 48 (2006) 2380-2405.
24. D. M. García-García, J. García-Antón, A. Igual-Muñoz, *Corros. Sci.*, 50 (2008) 2560-2571.
25. J.J. Xin, C. Fang, Y. T. Song, J. Wei, C. Huang, P. Libeyre, F. Simon, S. Sgobba, *IEEE T. Appl. Supercon.*, 27 (2017) 1-7.
26. L. Wang, N. Qiu, D. H. Hellmann, X. Zhu, *J. Mech. Sci. Technol.*, 30 (2016) 533-539.
27. W. Fu, Y. Zheng, X. He, *Wear*, 249 (2001) 788-791.
28. P. Niederhofer, F. Pöhl, K. Geenen, S. Huth, W. Theisen. *Tribol. Int.*, 95 (2016) 66-75.
29. K. H. Lo, C. T. Kwok, K. Y. Wang, W. Ai, *Wear*, 392 (2017) 159-166.
30. W. Tian, N. Du, S. Li, S. Chen, Q. Wu, *Corros. Sci.*, 85 (2014) 372-379.
31. P.C. Pistorius, G.T. Burstein, *Corros. Sci.*, 33 (1992) 1885-1897.
32. G.T. Burstein, R.M. Souto, *Electrochim. Acta*, 40 (1995) 1881-1888.
33. X. Bai X, D. B. Sun, H. Y. Yu, H. M. Meng, H. Q. Li, X. L. Zhang, *Chin. J. Nonferrous Met.*, 11 (2001) 285-289 (in Chinese)
34. J. H. Wu, K. P. Su, Y. Wang, W. J. Guo, *Sci. China Technol. Sci.*, 60 (2017) 523-528.